Supplementary Information

Droplet-based microfluidic synthesis of nanogels for controlled drug delivery: tailoring nanomaterial properties via pneumatically actuated flow-focusing junction

Sara Maria Giannitelli[a,†], Emanuele Limiti[a,†], Pamela Mozetic[b,c], Filippo Pinelli[d], Xiaoyu Han[e], Franca Abbruzzese[a], Francesco Basoli[a], Danila Del Rio[f], Stefano Scialla[a,g], Filippo Rossi[d], Marcella Trombetta[a], Laura Rosanò[f], Giuseppe Gigli[c,h], Zhenyu Jason Zhang[e], Emanuele Mauri[a,*], Alberto Rainer[a,c*]

[a] Department of Engineering, Università Campus Bio-Medico di Roma, via Álvaro del Portillo 21, 00128 Rome, Italy

[b] Division of Neuroscience, Institute of Experimental Neurology, San Raffaele Scientific Institute, Via Olgettina 60, 20132, Milan, Italy

[c] Institute of Nanotechnology (NANOTEC), National Research Council, via Monteroni, 73100, Lecce, Italy

[d] Department of Chemistry, Materials and Chemical Engineering "G. Natta", Politecnico di Milano, via L. Mancinelli 7, 20131 Milan, Italy

[e] School of Chemical Engineering, University of Birmingham, Edgbaston, Birmingham B15 2TT, UK

[f] Institute of Molecular Biology and Pathology, National Research Council (CNR), via degli Apuli 4, 00185 Rome, Italy

[g] National Institute of Chemical Physics and Biophysics, Akadeemia tee 23, 12618 Tallinn, Estonia

[h] Department of Mathematics and Physics "Ennio De Giorgi", Università del Salento, via per Arnesano, 73100 Lecce, Italy.

[†] *These authors equally contributed to this work.*

Doxorubicin calibration curve

Calibration solutions of DOX in PBS were prepared by two-fold serial dilution (down to 66 nM) starting from a 34 μM stock solution. Fluorescence measurements (λ_{ex} = 488 nm; λ_{em} = 590 nm) were recorded on a TECAN M200 spectrofluorometer. Calibration curve was obtained by plotting fluorescence levels *vs.* drug concentration and using a sigmoidal-based fitting of the experimental data (Figure S1).

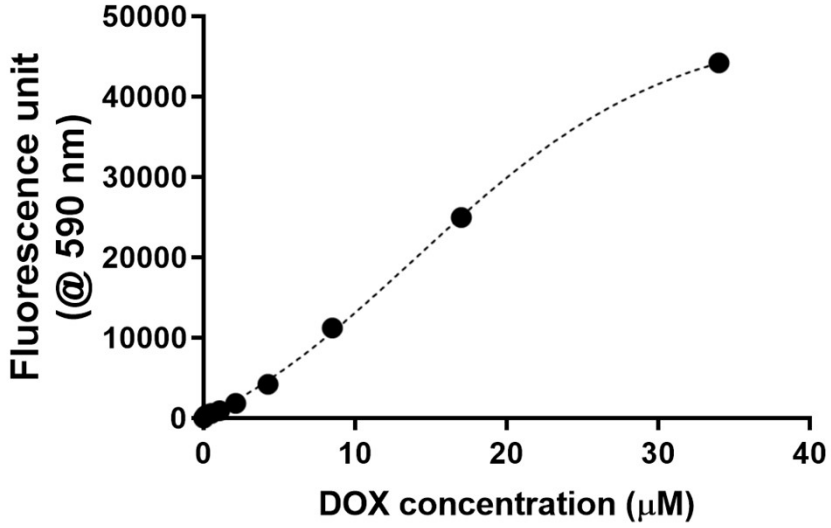

Figure S1. DOX calibration curve.

3D rendering of the tunable hydrodynamic flow focusing geometry

Figure S2 shows a representative 3D volume reconstruction of the hydrodynamic flow-focusing (HFF) geometry at different actuation levels (in the range in the range 0 – 2 bar), as obtained by confocal microscopy. The microfluidic channels were flooded with an aq. FITC solution and confocal micrographs were collected using a Nikon A1R+ laser scanning confocal microscope (Nikon Instruments, Tokyo, Japan) with a 20× NA 1.0 air objective.

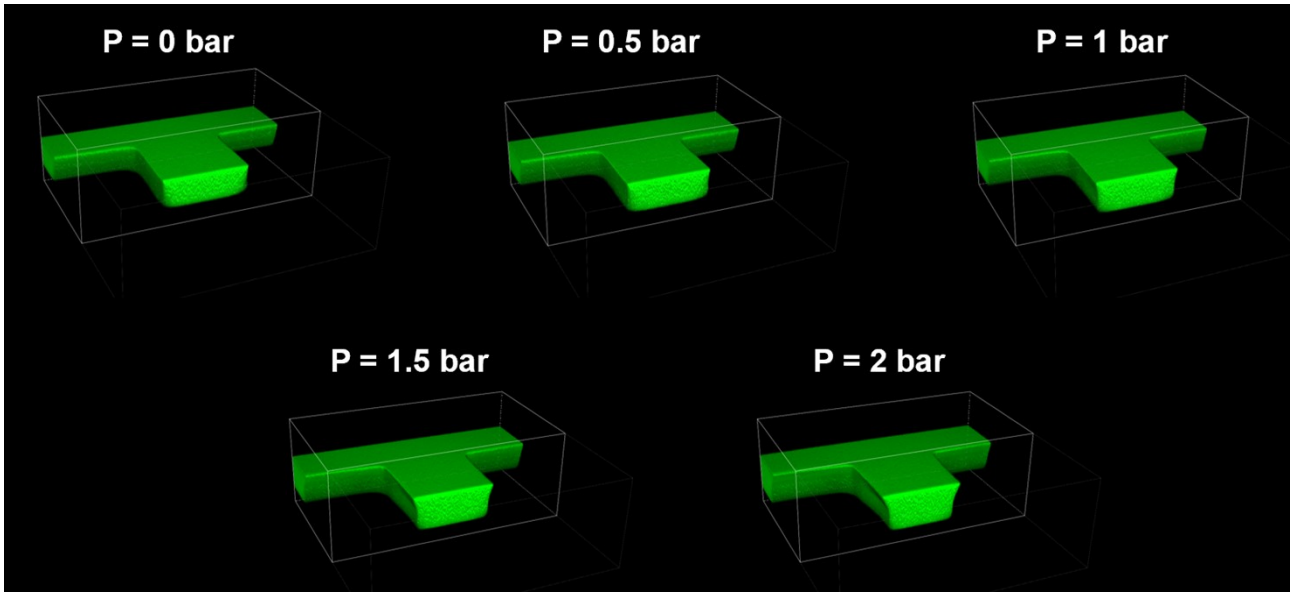

Figure S2. 3D volume reconstruction of the HFF junction at different pressure actuation levels.

Chemical crosslinking between HA and LPEI in microdroplets

To demonstrate that the formation of covalent bonds between HA and LPEI took place in each microdroplet and that the microfluidic pathway was necessary to form NGs, an aqueous solution of activated HA and LPEI was prepared in the same manner of the dispersed phase used in chip and left at room temperature up to 24 h. In this way, we reproposed the same reaction conditions for HA and LPEI, except for the microfluidic flow and droplet generation steps.

The polymeric solution was dialyzed (membrane MWCO = 6-8 kDa) against distilled water, for 3 days, with daily water change, in order to remove potential by-products. Finally, the resulting solution was freeze-dried and analyzed by ^{1}H-NMR.

Figure S3 shows the ^{1}H-NMR spectra of the *status* of HA-LPEI solution after 24 h, compared to the spectrum of obtained NGs (NG_0, as a representative specimen). In all spectra of the bulk polymeric solution, the signals corresponding to the covalent crosslinking were missing. In particular, the characteristic shift (3.39 ppm) of LPEI peaks were not detectable. This result confirmed that the covalent linkage between the two polymers was conceivably favored by the diffusion mixing, the convective transport and the flow field inside the forming microdroplets[1-3], and, as a result, the NGs were produced.

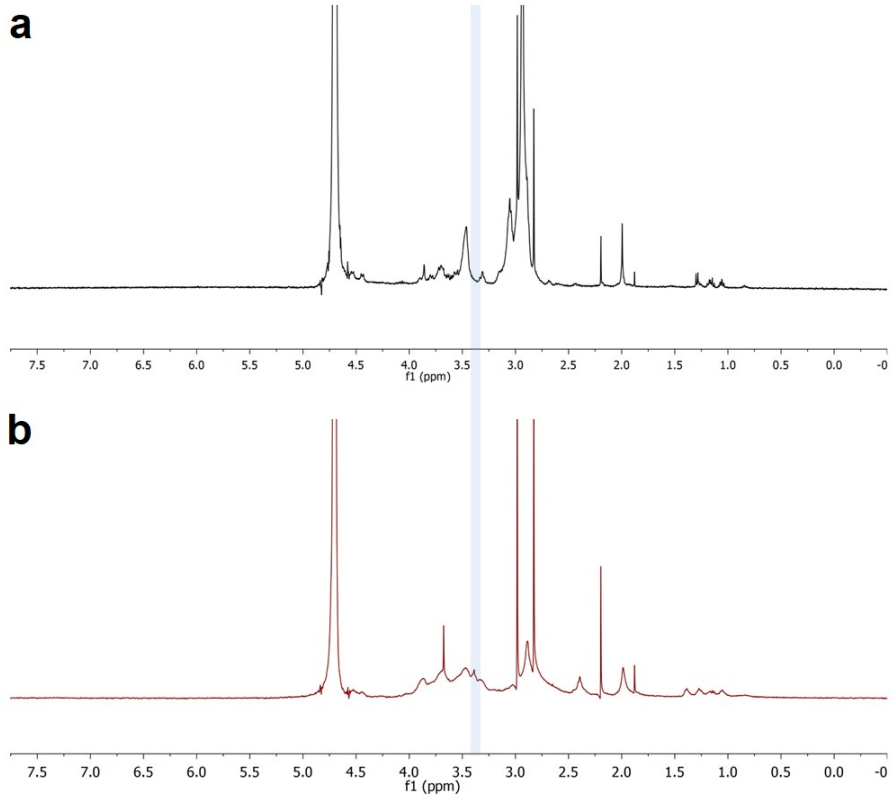

Figure S3. (a) ^{1}H-NMR spectrum of the HA-LPEI solution equal to the dispersed phase used in droplet-based microfluidics, left at room temperature for 24 h without implementation in microfluidic steps and dialyzed. Compared to NGs spectrum (b, NG_0), the signals of chemical crosslinking HA-LPEI are missing (as highlighted in the blue area).

DLS comparison between conventional W/O emulsion and microfluidic NG syntheses

NGs obtained via our microfluidic strategy (i.e., NG_0 and NG_2) were characterized by DLS and contrasted with NGs produced *via* a standard W/O emulsion batch process (NG_b): the main differences in size and PDI related to the two synthetic routes are reported in Figure S4. In detail, NG_b were synthetized using the same polymer solution of the droplet-based microfluidic approach, following these steps: LPEI-Cy5 (6.8 mg, 2.7 μmol) and pristine LPEI (6.8 mg, 2.7 μmol) were dissolved in dilute HCl (1.5 mL, pH = 4.5), then added dropwise to the solution of activated HA (1.5 mL), and vortexed for 1 min. The resulting system represented the aqueous phase. The organic phase was 3% w/v Span 80 in mineral oil (5 mL). Finally, the polymer solution (1 mL) was added dropwise to the organic phase, under stirring, and the obtained W/O emulsion was stirred for 8 h. NGs were collected as a powder after extraction with diethyl ether, dialysis against DIW and freeze-drying, as discussed in the microfluidic synthesis of NG_0 and NG_2.

As shown in Table S1, NG_b was characterized by higher values of mean hydrodynamic diameter (D) and polydispersity index (PDI) than NGs obtained *via* microfluidics: this confirmed the high potential of the microfluidic platform to control the NG synthesis and to produce nanoparticles with extremely reproducible size.

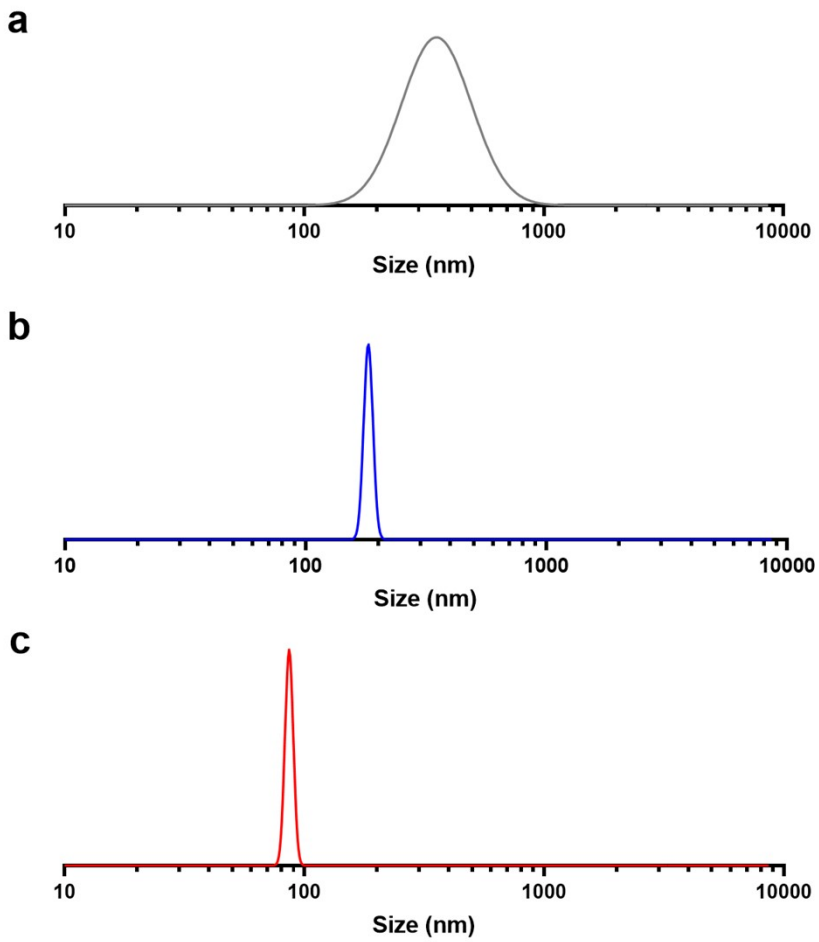

Figure S4. DLS graphs of NG_b (a, black), NG_0 (b, blue) and NG_2 (c, red).

Table S1. DLS analysis of NGs specimens.

	D (nm)	**PDI (-)**
NG_b	342.1	0.193
NG_0	188.3	0.023
NG_2	92.4	0.015

Furthermore, DLS analysis indicated that NG_0 and NG_2 did not show significant coalescence and aggregation in PBS, preserving their size as reported in Figure S5.

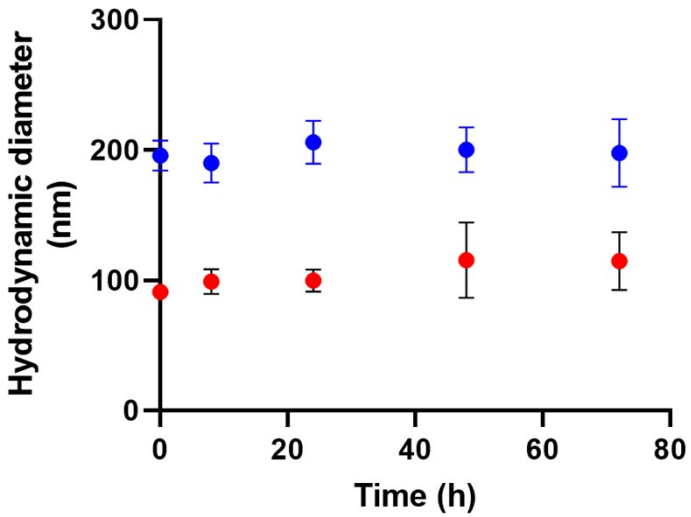

Figure S5. Stability of NG_0 (blue) and NG_2 (red) specimens in PBS. The experiments were performed in triplicate.

Drug release by NGs produced through conventional W/O emulsion (NG_b)

NG_b was tested as a reference drug delivery system for our NG_0 and NG_2 specimens, to highlight the different performances between the traditional NG synthesis and our innovative microfluidic production. Drug loading and release study were performed as discussed in the main text. Briefly, 30 μL of a 100 μM DOX solution were added to lyophilized NG_b (3 mg) and left at RT for 15 min; the encapsulation efficiency was estimated following dialysis against PBS (30 min). The resulting DOX-loaded NGs were diluted to a final concentration of 10 mg/mL and 100 μL of the suspension were allowed to exchange against PBS, withdrawing aliquots at defined time points to determine the eluted drug concentration by fluorescence spectroscopy (λ_{ex} = 488 nm, λ_{em} = 590 nm). NG_b was characterized by *ca.* 70% drug loading and exhibited an almost completed drug release in the first 6 h (Figure S6), which results faster than DOX/NG_0 and DOX/NG_2 specimens (*ca.* 74.5% and 63% after 6 h, respectively). This different trend could be presumably correlated to the different composition of NG_b, characterized by a LPEI:HA molar ratio 2.5:1. The lower amount of glycosaminoglycan than in NG_0 and NG_2 could affect the aliphatic-aromatic stacking between DOX and HA. Consequently, the reduced drug-polymer interactions could justify the experimentally determined faster release of DOX compared to the microfluidic-templated NGs. Moreover, plotting the drug release against time to the power of 0.43 (i.e., $t^{1/2.3}$), a linear trend was clearly recognizable, suggesting that DOX release was mediated by Fickian diffusion regime, as in NG_0 and NG_2.

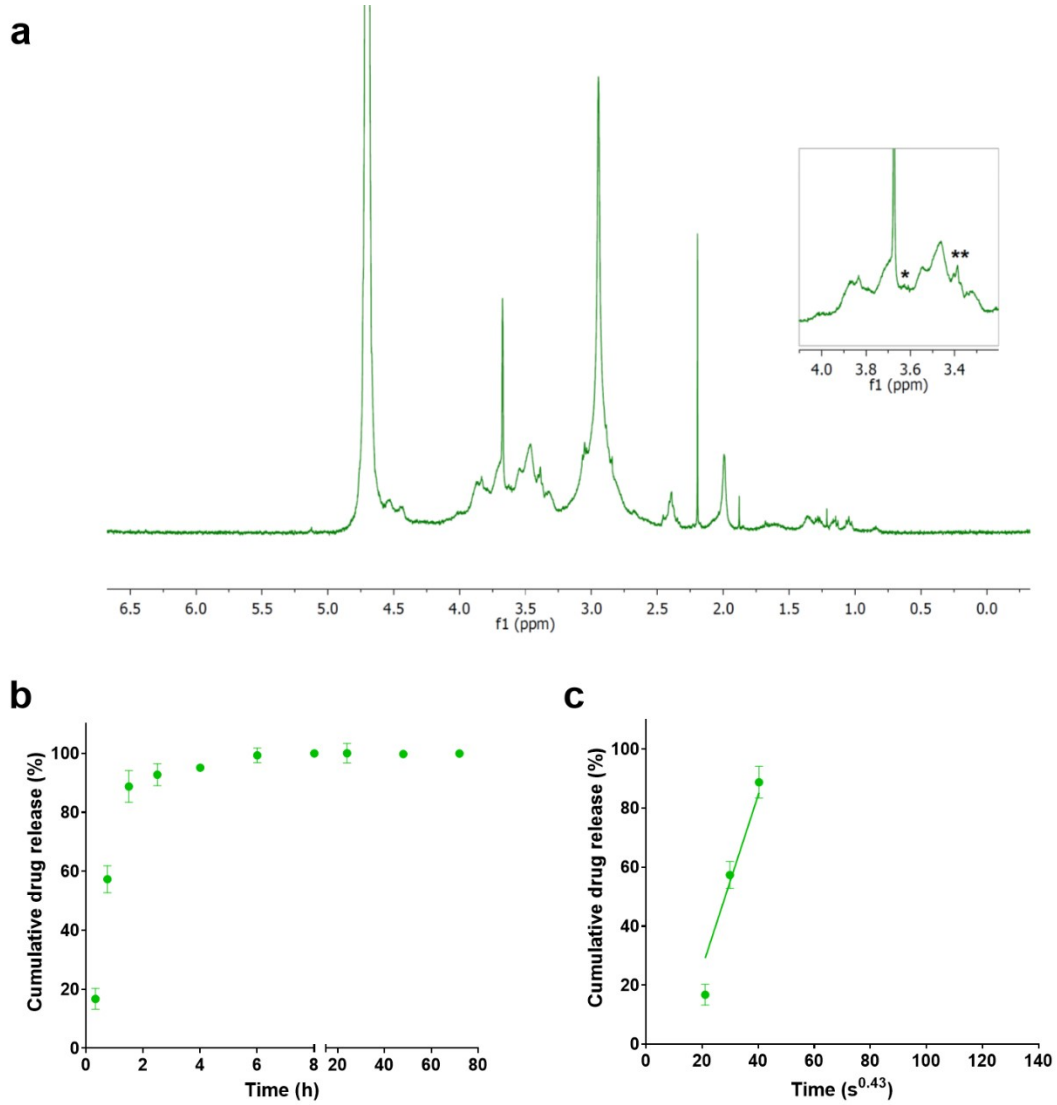

Figure S6. (a) ^{1}H-NMR spectrum of NG_b: the characteristic signals of HA-LPEI crosslinking (* and **) are highlighted. (b) DOX release profile by NG_b. (c) The slope of the drug release against time expressed as $t^{1/2.3}$ is representative of the Fickian diffusion coefficient of the drug in NGs. Cumulative drug release is represented as a percentage of the total drug payload (mean value ± SD is plotted).

Overall, these results confirmed that NG_0 and NG_2 were more efficient nanocarriers than NG_b, and eligible as controlled drug delivery systems for therapeutic applications.

Cytotoxicity and metabolic effects of DOX release from NG_b specimens.

Cytotoxicity of NG_b and the potential therapeutic effect of NG_b-mediated release of DOX were evaluated using G6PD and MTT assays, respectively. The specimens were administered to OVCA433 cells following the procedures described in the manuscript. As shown in Figure S7, NG_b was not cytotoxic (cell viability close to 99%). However, the therapeutic effect of DOX/NG_b treatment was lower than in DOX/NG_0 and DOX/NG_2 (77 % residual viability for DOX/NG_b *vs*. 18 % for DOX/NG_0 and 5 % for DOX/NG_2 after 1 week), indicating that the NGs synthetized by droplet-based microfluidics were more effective as DOX nanocarriers compared to NGs obtained by conventional W/O emulsion.

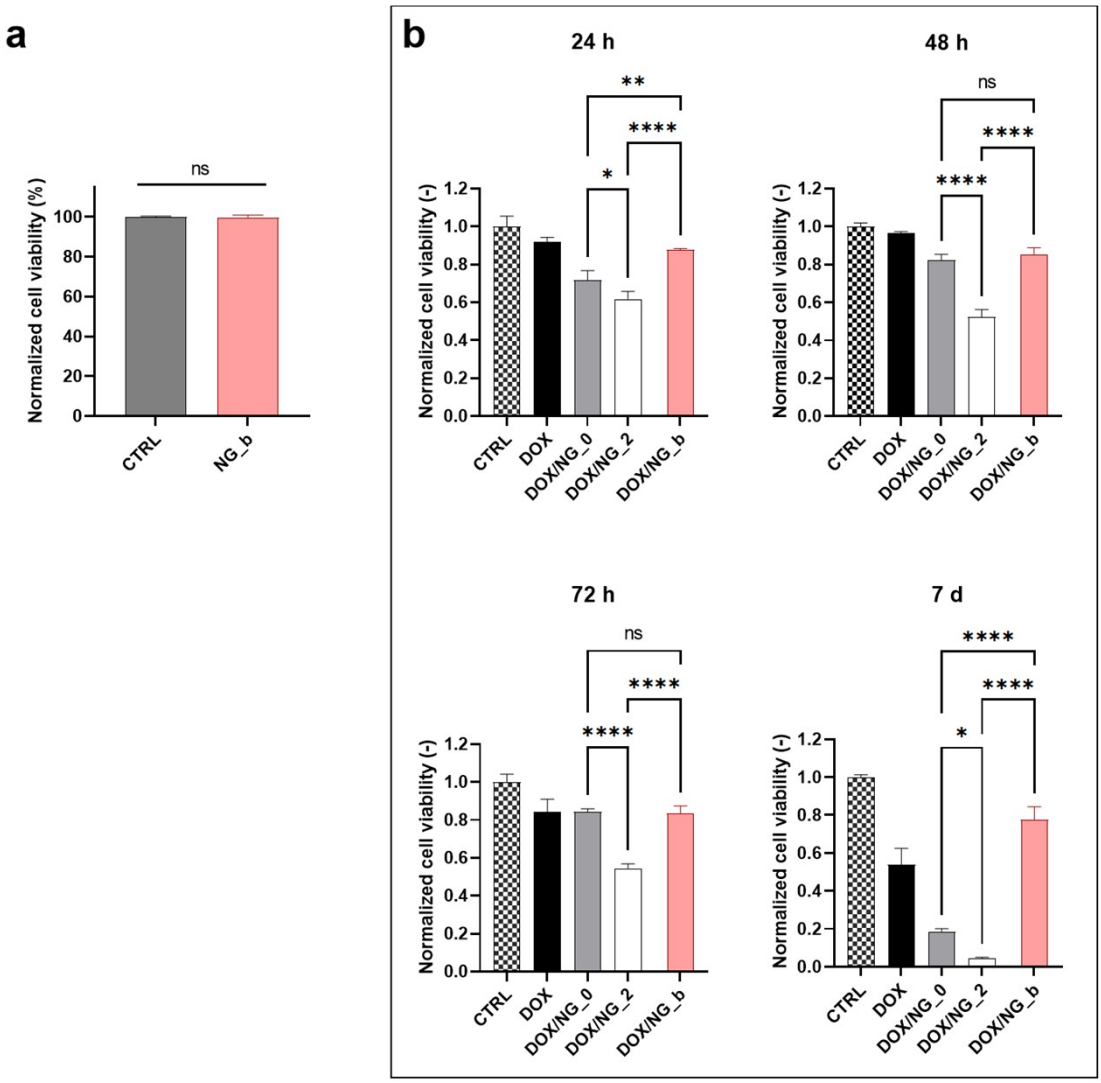

Figure S7. (a) Cytocompatibility of pristine NG_b by G6PD assay. Viability levels were normalized to CTRL group and expressed as mean ± SD. (b) Comparison of the cytotoxic effect in OVCA433 of DOX/NG_b (in

red) vs DOX-loaded microfluidic-templated NGs, at 24 h, 48 h, 72 h and 7 days. For the sake of clarity, we reported the data discussed in the main text and we displayed the comparisons among the NG-based treatments. Groups refer to a 30 min incubation with the NGs. The therapeutic effect is expressed in terms of cell viability levels normalized against their internal controls, measured through the MTT assay. Results are the mean ± SD. Statistical analysis was performed using one-way ANOVA. * $p < 0.05$, ** $p < 0.01$, *** $p < 0.001$, **** $p < 0.0001$, ns = not significant.

References

1. R. Seemann, M. Brinkmann, T. Pfohl and S. Herminghaus, *Rep Prog Phys*, 2011, **75**, 016601.
2. O. Carrier, F. G. Ergin, H.-Z. Li, B. B. Watz and D. Funfschilling, *J Micromech Microeng*, 2015, **25**, 084014.
3. J. D. Tice, H. Song, A. D. Lyon and R. F. Ismagilov, *Langmuir*, 2003, **19**, 9127-9133.